EVALUATION OF DAMAGE INITIATION MODELS FOR 3D-WOVEN FIBRE COMPOSITES

Carolyn Oddy[1], Tomas Ekermann[2], Magnus Ekh[1], Martin Fagerström[1] and Stefan Hallström[2]

[1]Division of Material and Computational Mechanics, Department of Industrial and Materials Science, Chalmers University of Technology, SE-412 96 Gothenburg, Sweden
[2]Department of Aeronautical and Vehicle Engineering, KTH Royal Institute of Technology, SE-100 44 Stockholm, Sweden
Email: carolyn.oddy@chalmers.se, tomla@kth.se, magnus.ekh@chalmers.se, martin.fagerstrom@chalmers.se, stefanha@kth.se

Keywords: 3D-woven reinforcement, finite element modelling, damage initiation

Abstract
Three dimensional (3D) fibre-reinforced composites have shown weight efficient strength and stiffness characteristics as well as promising energy absorption capabilities. In the considered class of 3D-reinforcement, vertical and horizontal weft yarns interlace warp yarns. The through-thickness reinforcements suppress delamination and allow for stable and progressive damage growth in a quasi-ductile manner. With the ultimate goal of developing a homogenised computational model to predict how the material will deform and eventually fail under loading, this work proposes candidates for failure initiation criteria. The criteria are evaluated numerically for tensile, compressive and shear tests. The extension of the LaRC05 stress based failure criteria to this class of 3D-woven composites is one possibility. This however, presents a number of challenges which are discussed. These challenges are related to the relative high stiffness in all directions, which produce excessively high shear components when projected onto potential off-axis failure planes. To circumvent these challenges, strain based criteria inspired by LaRC05 are formulated. Results show that strain based failure predictions for the simulated load cases are qualitatively more reasonable.

1. Introduction

With the European Union's introduction of strict emissions limits, the race to manufacture increasingly energy efficient vehicles is well underway. The traditional use of laminated fibre composites, in particular carbon fibre reinforced polymers (CRFP), provide high stiffness and strength relative to weight. Laminated composites also provide high specific energy absorption capabilities when certain conditions are met. Specifically that a pertinent deformation mode is triggered and delaminations are suppressed. However, in the event that delamination cracks form and propagate, much of the material's energy absorption capability is lost as this damage mode consumes less energy than e.g. a fibre kinking process. This behaviour presents challenges when it comes to using traditional laminated fibre composites in certain vehicle components, such as those that must absorb energy and undergo excessive bending.

A recently introduced class of composites with three dimensional (3D) woven reinforcement, show a number of positive characteristics. As the name suggests, yarns are interlaced in three principal directions wherein vertical and horizontal weft yarns interlace warp yarns. The weaving technique allows for direct manufacturing of complex geometries with minimal material waste. The fibre network also prevents delamination and inhibits crack growth. This means that 3D fibre-reinforced composite structures are able to maintain their load carrying capacity under extreme bending, unlike their laminated counterparts. As well as having weight efficient strength and stiffness characteristics, 3D-CFRP beams

have shown promising energy absorption capabilities by Kazemahvazi et al.[1] and Khokar et al. [2]. Specifically, Khokar et al. have shown that, in bending, a 3D-CFRP I-beam has two to three times the specific energy absorption capability of a steel beam with equivalent geometry, see Fig. 1. The specific load - displacement curves of the two I-beams under four point bending are given. The 3D-CFRP beam exhibits a quasi-ductile failure with a considerable load carrying capacity remaining after initial failure. The through-thickness reinforcements suppress delamination and allow damage to grow in a stable and progressive manner.

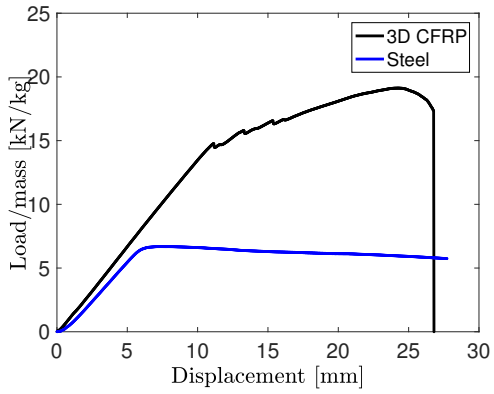

Figure 1: Specific load - displacement curves of a 3D-CFRP and Steel I-Beam with the same dimensions under four point bending. From Khokar et al. [2].

As the concept design for future vehicles is largely simulation driven, the long-term objective is to develop a computationally efficient homogenised material model for 3D fibre-reinforced composites. Such a model must be capable of describing how the 3D fibre-reinforced composites deform and eventually fail under loading. In particular, it must predict the damage process that leads to energy absorption. As a starting point, it is essential that activation of the non-linear damage process is predicted with sufficient accuracy. To find suitable damage activation criteria, failure (or design) criteria initially developed for uni-directional (UD) fibre composites are adopted in this paper. Specifically LaRC05 [3] is extended to the considered class of 3D fibre-reinforced material. This stress based approach however presents a number of challenges due to the high relative stiffness of the 3D-reinforcement in all directions. As an alternative, a strain based approach inspired by LaRC05 is also presented, which proves more successful. Note that, long term, these criteria should serve as damage initiation criteria thus indicating the onset of non-linear, irreversible and stiffness degrading mechanisms in the material. Currently however, we will evaluate their qualitative performance as design criteria with load cases made to determine the strength of a CFRP with 3D-woven reinforcement, the future goal being to compare the results to experiments.

2. 3D Fibre-Reinforcement Architecture

A sketch of a typical construct of this class of 3D-woven reinforcement is presented in Fig. 2. It consists of three sets of yarns: warp yarns (blue) extending in the weaving direction as well as horizontal weft (red) and vertical weft (green) yarns extending transversely to the weave in the width and thickness directions respectively.

During the weaving process, warp yarns are alternately interlaced with horizontal and vertical weft yarns in a grid-like set. The weaving process, developed by Khokar, is described in [4]. The material that has been used for verification in this paper was presented and tested by Ekermann et al. [5]. It consists of 3D-woven carbon fibre reinforcements that have been impregnated with RTM6 epoxy. The 3D-reinforcement is woven

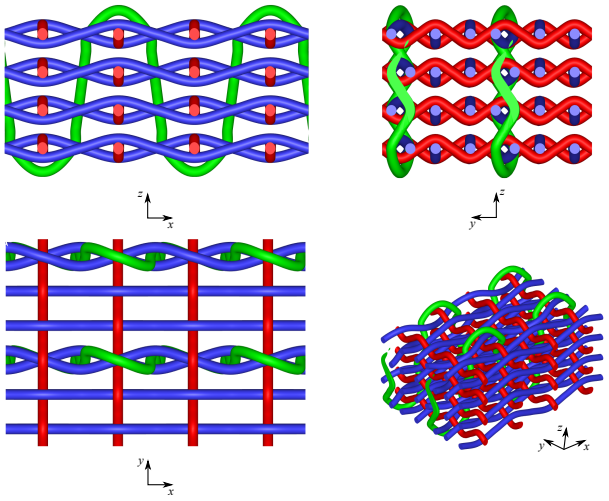

Figure 2: Sketches of the 3D-woven reinforcement, created in TexGen [6]. Blue yarns are warp, green and red yarns are horizontal and vertical weft.

with a vertical weft yarn on every third column in the warp matrix cf. Fig. 2.

Mechanical properties of the material are presented in Table 1. They have been estimated using values taken from Ekermann et al. [5] and on weave parameters. Note that the material directions, namely warp, horizontal weft and vertical weft are denoted by x, y and z respectively. Future experiments will be performed to identify more accurate parameter values. Current estimations are used to qualitatively evaluate the predictions of the failure criteria.

Table 1: Material parameter values. X_T, X_C, S_{xy}, S_{xz} and S_{yz} are taken from [5]. Other properties have been been estimated from weave parameters (fibre content, crimp, etc.) and properties of the fibres and matrix.

Stiffness	E_x	88 [GPa]	E_y	30 [GPa]	E_z	17 [GPa]
Shear stiffness	G_{xy}	3.2 [GPa]	G_{xz}	3.4 [GPa]	G_{yz}	2.3 [GPa]
Poisson's ratio	ν_{xy}	0.16	ν_{xz}	0.25	ν_{yz}	0.33
Tensile strength	X_T	929 [MPa]	Y_T	220 [MPa]	Z_T	180 [MPa]
Compressive strength	X_C	360 [MPa]	Y_C	255 [MPa]	Z_C	235 [MPa]
Shear strength	S_{xy}	60 [MPa]	S_{xz}	90 [MPa]	S_{yz}	48 [MPa]

3. Extending LaRC05 to 3D Fibre-Reinforced Composites

The LaRC05 failure criteria has been widely adopted to predict failure initiation and propagation in fibre-reinforced composites consisting of UD plies subjected to a 3D-stress state. It uses three failure indices to predict tensile fibre failure, matrix dominated failure, and compressive fibre failure due to fibre kinking or splitting. The pertinent failure mode is assumed to initiate when the index reaches a value of one. The extension and perhaps minor modification of the LaRC05 criteria to 3D fibre-reinforced composites could prove positive. A natural first step in this extension would be the assumption of three independent, superimposed fibre directions, which can each be simultaneously checked for fibre tensile failure, matrix failure and fibre kinking/ splitting. In fact, a similar approach has been used by Juhasz et al. [7] when predicting failure of a composite consisting of in-plane UD layers with vertical reinforcement.

Tensile fibre failure, is predicted using the maximum stress criterion by LaRC05. Extending this to three mutually perpendicular fibre directions gives the following failure indices:

$$FI^x_{FT} = \frac{\langle \sigma_x \rangle}{X_T}, \quad FI^y_{FT} = \frac{\langle \sigma_y \rangle}{Y_T}, \quad FI^z_{FT} = \frac{\langle \sigma_z \rangle}{Z_T}, \quad \langle \bullet \rangle = max\{0, \bullet\}, \tag{1}$$

where X_T, Y_T and Z_T denote the tensile strength in the x, y and $z-$directions. Recall, that they signify the warp, horizontal weft and vertical weft respectively.

To predict matrix dominated failure under multi-axial loading, a modified version of the Mohr-Coulomb failure criterion is adopted. It is assumed that matrix failure is governed by stress interaction in the fracture plane, illustrated in Fig. 3 for a UD laminate. The stress components τ_T, τ_L and σ_N (see Fig. 3) are obtained through a stress transformation based on the angle $0° \leq \alpha \leq 180°$, that maximises FI_M, given by

$$FI_M = \left(\frac{\tau_T}{S_T - \eta_T \sigma_N} \right)^2 + \left(\frac{\tau_L}{S_L - \eta_L \sigma_N} \right)^2 + \left(\frac{\langle \sigma_N \rangle}{Y_T} \right)^2. \tag{2}$$

Failure is therefore assumed to occur when the shear and normal stresses overcome their respective strengths, denoted by S_T, S_L and Y_T. The friction coefficients η_T and η_L are introduced in order to account for increased shear strength under the presence of compressive normal loading as well as decreased strength under tensile normal loading. Extending LaRC05 to consider three independent matrix

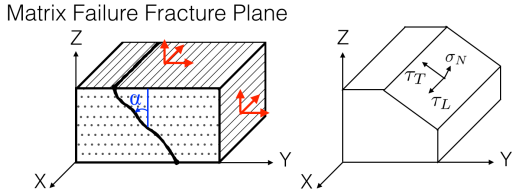

Figure 3: Illustration of LaRC05 UD matrix failure criteria.

failure indices would require checking for stress interactions, using Eq. (2), in three fracture planes rotated around each fibre axis.

Using LaRC05 in this manner however, is not so straightforward. The relative high stiffness in all fibre directions creates artifacts when the criterion is used in this way. It is perhaps best illustrated by considering the material under uniaxial tensile loading in the warp (x) direction. The three failure indices, given by FI^x_M, FI^y_M, FI^z_M and their related failure planes are illustrated in Fig. 4.

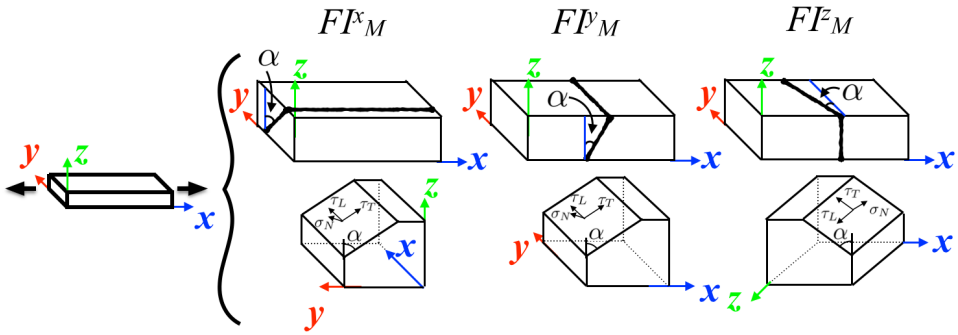

Figure 4: Considered matrix failure planes of 3D-reinforced composite.

Fig. 5 shows the stress components in the fracture plane around y for varying α. Likewise, Fig. 5 also shows the failure index value computed according to Eq. (2). For simplicity it is assumed that $S_T = S_L = S_{xz}$ and $\eta_T = \eta_L = 0.3$. The stresses are taken when tensile fibre failure is predicted in the warp direction, i.e. when $\sigma_x = X_T$. Note that due to the high stiffness in the warp direction, large stress components are found in the fracture plane for certain angles.

This leads directly to a number of challenges. Firstly, the normal stress for small (and large) angles, is substantially larger than the most favourable shear strength of the material, even when scaled by η_T. As σ_N decreases, a specific angle will eventually give $S_T - \eta_T \sigma_N = 0$, driving the failure index to infinity.

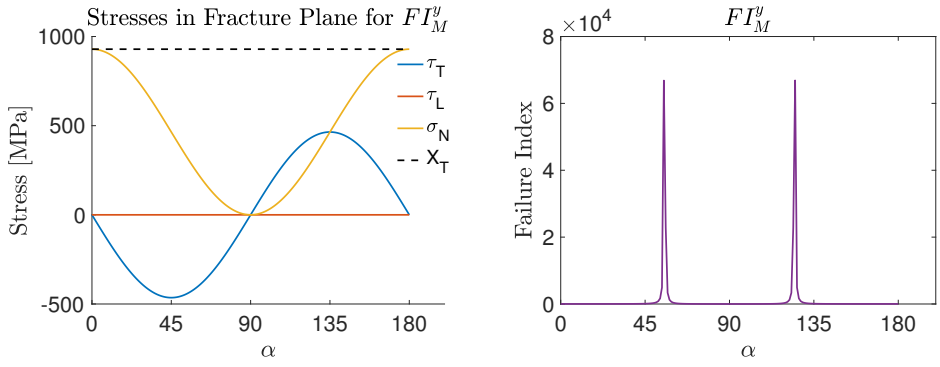

Figure 5: Stresses in the fracture plane (left) and failure index (right) around y computed according to Eq. (2).

This behaviour is resolved by returning to a failure indicator that resembles that presented in LaRC04 [8]. That is, it is assumed that only compressive normal stresses affect the shear strength. Note also, that due to the material characteristics, the normal strength in the fracture plane should vary depending

on α. The following modification may then be proposed:

$$FI_M^y = \left(\frac{\tau_T}{S_T + \eta_T\langle -\sigma_N\rangle}\right)^2 + \left(\frac{\tau_L}{S_L + \eta_L\langle -\sigma_N\rangle}\right)^2 + \mathcal{H}(\sigma_N)\left(\left(\frac{\sigma_{Nx}}{X_T}\right)^2 + \left(\frac{\sigma_{Nz}}{Z_T}\right)^2\right), \quad (3)$$

where $\mathcal{H}(\bullet)$ denotes the Heaviside step function and σ_{Nx} and σ_{Nz} signify the projection of the normal stress onto the warp and vertical weft directions. Fig. 6 shows the resulting matrix failure index around y for varying α when $FI_{FT}^x = 1$. Even though the problem with infinite values of the failure criterion is now resolved, extending LaRC05 in this manner leads to unrealistic predictions of early matrix failure. This is explained by shear stresses in the fracture plane which are substantially larger than the shear strengths.

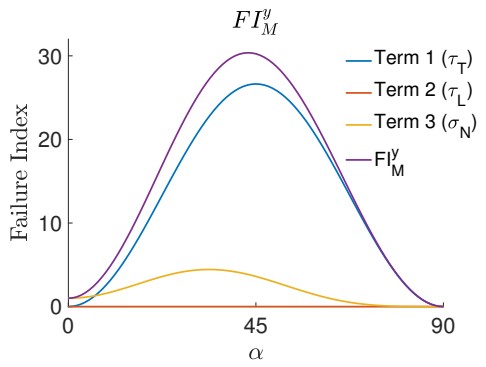

Figure 6: Illustration of LaRC05 UD matrix failure criteria.

The final failure index used by LaRC05 allows for the prediction of fibre compression failure, either by fibre kinking or splitting. It is assumed that compressive fibre failure is a result of shear-dominated matrix failure in a misalignment frame. Extending this failure index in a similar manner to the 3D fibre-reinforced composite, presents similar challenges due to the high stiffness in all directions.

4. Strain-Based Criteria

4.1. Formulation

In order to circumvent the artifacts discussed in Section 3, strain based failure indices in the spirit of LaRC05 are instead proposed. Specifically, a maximum strain criteria in tension and compression in the three fibre directions, as well as a LaRC05 based matrix failure criterion are introduced. That is, for tensile and compressive failure in the fibre directions:

$$FI_{FT,\epsilon}^x = \frac{\langle \epsilon_x\rangle}{X_{T,\epsilon}}, \quad FI_{FT,\epsilon}^y = \frac{\langle \epsilon_y\rangle}{Y_{T,\epsilon}}, \quad FI_{FT,\epsilon}^z = \frac{\langle \epsilon_z\rangle}{Z_{T,\epsilon}}, \quad (4)$$

$$FI_{FC,\epsilon}^x = \frac{\langle -\epsilon_x\rangle}{X_{C,\epsilon}}, \quad FI_{FC,\epsilon}^y = \frac{\langle -\epsilon_y\rangle}{Y_{C,\epsilon}}, \quad FI_{FC,\epsilon}^z = \frac{\langle -\epsilon_z\rangle}{Z_{C,\epsilon}}, \quad (5)$$

where the allowable tensile and compressive strains in the three fibre directions are denoted by $X_{T,\epsilon}$, $Y_{T,\epsilon}$, $Z_{T,\epsilon}$, $X_{C,\epsilon}$, $Y_{C,\epsilon}$ and $Z_{C,\epsilon}$ respectively. Additionally, the three considered matrix failure indices are computed as

$$FI_{M,\epsilon}^x = \left(\frac{\gamma_T}{S_{T,\gamma} + \eta_{T,\gamma}\langle -\epsilon_N\rangle}\right)^2 + \left(\frac{\gamma_L}{S_{L,\gamma} + \eta_{L,\gamma}\langle -\epsilon_N\rangle}\right)^2 + \mathcal{H}(\epsilon_N)\left(\left(\frac{\epsilon_{Ny}}{Y_{T,\epsilon}}\right)^2 + \left(\frac{\epsilon_{Nz}}{Z_{T,\epsilon}}\right)^2\right), \quad (6)$$

$$FI_{M,\epsilon}^y = \left(\frac{\gamma_T}{S_{T,\gamma} + \eta_{T,\gamma}\langle -\epsilon_N\rangle}\right)^2 + \left(\frac{\gamma_L}{S_{L,\gamma} + \eta_{L,\gamma}\langle -\epsilon_N\rangle}\right)^2 + \mathcal{H}(\epsilon_N)\left(\left(\frac{\epsilon_{Nx}}{X_{T,\epsilon}}\right)^2 + \left(\frac{\epsilon_{Nz}}{Z_{T,\epsilon}}\right)^2\right), \quad (7)$$

$$FI_{M,\epsilon}^z = \left(\frac{\gamma_T}{S_{T,\gamma} + \eta_{T,\gamma}\langle -\epsilon_N\rangle}\right)^2 + \left(\frac{\gamma_L}{S_{L,\gamma} + \eta_{L,\gamma}\langle -\epsilon_N\rangle}\right)^2 + \mathcal{H}(\epsilon_N)\left(\left(\frac{\epsilon_{Nx}}{X_{T,\epsilon}}\right)^2 + \left(\frac{\epsilon_{Ny}}{Y_{T,\epsilon}}\right)^2\right). \quad (8)$$

Here, $S_{T,\gamma}$ and $S_{L,\gamma}$ signify the allowable engineering shear strain. Again the strain components γ_T, γ_L and ϵ_N are obtained for each failure index by strain transformations based on $0° \leq \alpha \leq 180°$, illustrated in Fig. 4, that maximises each respective failure index. Note that the stresses have been replaced by their corresponding strains.

4.2. Results and Discussion

As previously discussed, the long term application of these criteria is to indicate the onset of irreversible and non-linear stiffness degradation mechanisms in the material. Currently, their performance is evaluated qualitatively against tests used to determine the strength of the 3D-CFRP. Specifically uniaxial tension and compression in the warp direction as well as in-plane shear. In this respect, the failure indices are evaluated as design criteria for the time being. It is assumed that strain limits can be modified in the future however, to predict failure initiation rather than final failure.

The allowable strain values are estimated as the ratios between the strength and stiffness in each direction. Note that in general the allowable shear strains are dependent on the fracture angle. However, for simplicity, the following material parameters are adopted:

$$\begin{gathered} X_{T,\epsilon} = Y_{T,\epsilon} = Z_{T,\epsilon} = 0.01, \\ \mathrm{X}_{C,\epsilon} = 0.004, \quad Y_{C,\epsilon} = 0.012, \quad Z_{C,\epsilon} = 0.014 \\ \mathrm{S}_{T,\epsilon} = S_{L,\epsilon} = 0.02. \end{gathered}$$

Tensile loading along the warp direction of a flat edged sample, predicts fibre tensile failure to be most critical, see Fig. 7. Unlike its stress based counterpart, matrix failure is no longer predicted excessively early. Matrix failure is primarily driven by the normal strains in the fracture plane at small and large angles. In this respect, the final terms in Eqs. (6), (7) and (8) behave in a manner resembling the maximum strain criteria. Likewise, Fig. 8 shows the evolution of the failure criteria under compressive loading in the warp direction. Compressive failure, indicated by the maximum strain criterion in the warp direction, dominates.

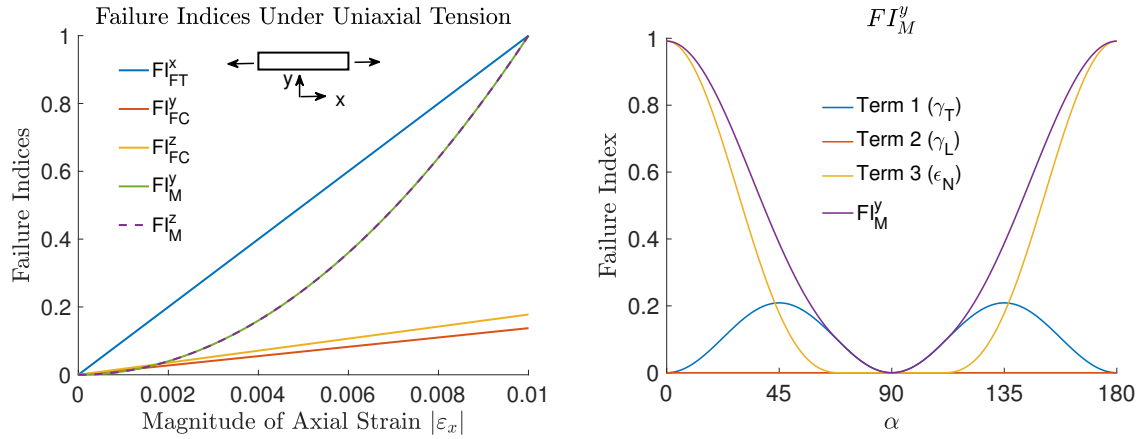

Figure 7: Evolution of failure criteria under uniaxial tension (left) and FI^y_M with contributions from each term (right).

The behaviour of the material under in-plane shear is investigated using the specimen illustrated in Fig. 9. The evolution of the damage criteria for the indicated red point in the shear dominated region is also shown. Matrix failure around z is predicted as the critical failure mechanism. The variation of FI^z_M as well as the fracture angle along the shear dominated region are plotted in Fig. 10. A contour plot of

FI_m^z over the shear specimen is also shown with a sketch of the fracture angles around z. Note that the aforementioned sampling point is indicated. Failure is predicted first in the rightmost stress concentration before initiating in the leftmost stress concentration and propagating inwards.

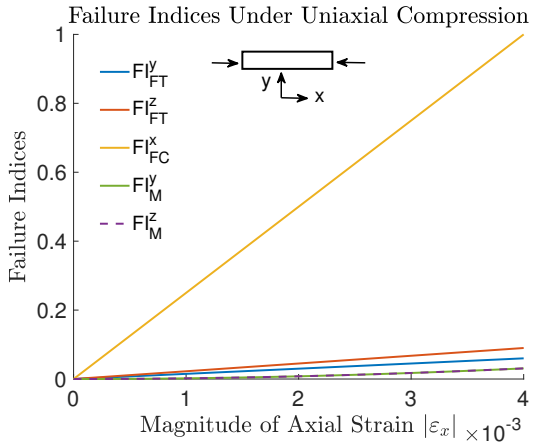

Figure 8: Evolution of failure criteria under uniaxial compression.

Fracture initiates at angles between 138° to 145°. As illustrated, this strain based failure criterion predicts the formation and likely the eventual coalescence of inclined cracks along the shear dominated region. This can be seen as a phenomenon synonymous to the formation of cusps in e.g. mode II shear loading [9].

The strains in the fracture plane and the contributions from each term in FI_m^z for varying fracture angles are plotted in Fig. 11. They are again shown for the indicated point. Failure is driven by the normal strains, ϵ_N. This is again similar to the mechanisms that form cusps, i.e. pure shear loading giving rise to principal tensile stresses at an angle of $45°$ which lead to inclined crack development.

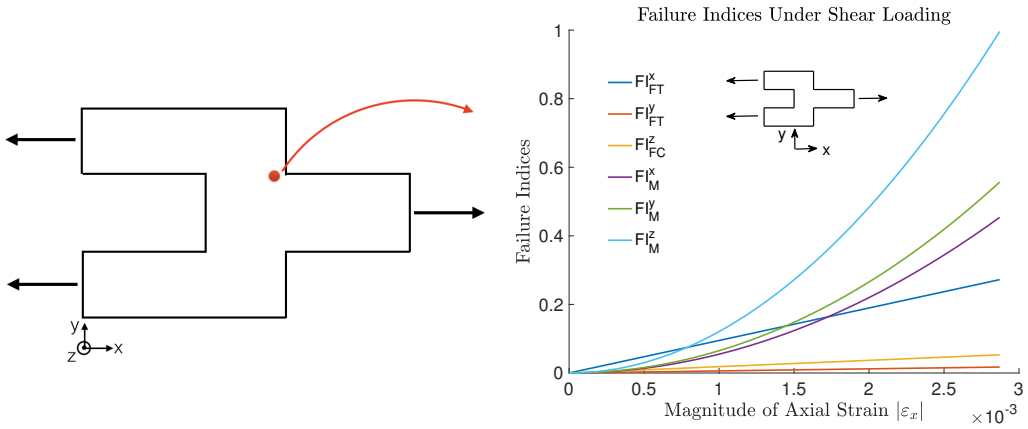

Figure 9: Illustration of shear specimen (left) and evolution of failure criteria at the indicated point (right).

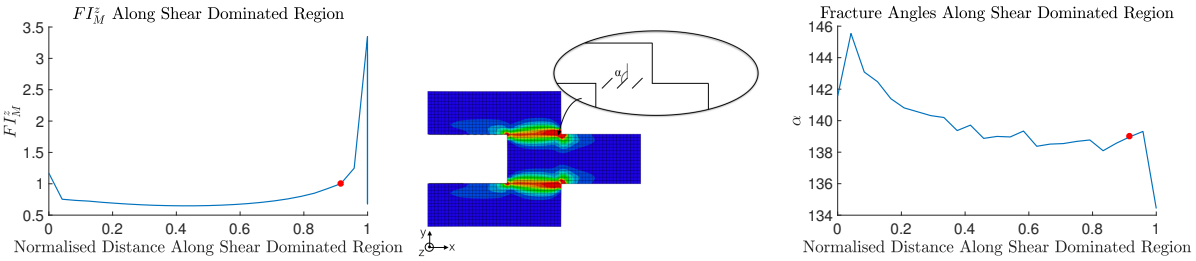

Figure 10: Variation of FI_M^z along the shear dominated region (left), contour plot of FI_M^z with indicated fracture angle (middle) and the variation of fracture angle along shear region (right). The sampling point used to generate Fig. 9 is indicated with a red dot.

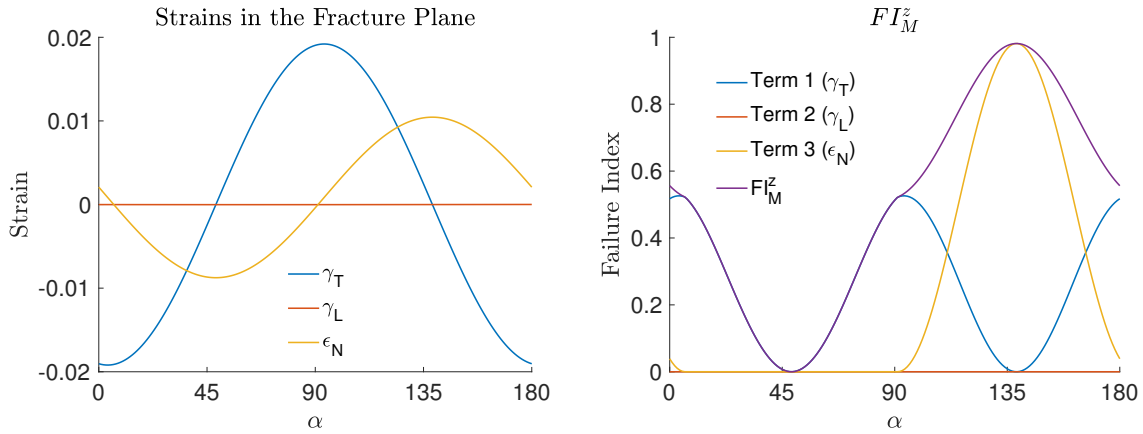

Figure 11: Strain components in the fracture plane (left) and FI_M^z with contributions from each term (right) for varying α.

5. Conclusions and Outlook

Results from strain based criteria applied to this class of 3D-reinforced composites seem qualitatively more reasonable for failure predictions when compared to stress based criteria of a similar form. Unlike their UD counterparts, shear failure of this 3D-woven composite is not strictly governed by matrix failure. It also requires the breaking of fibre bundles. For this reason it is possible that homogenised deformations better represent the load carrying interaction and failure of the matrix and fibre bundles. Predictions will be validated with future experiments as well as mesoscale modelling of the 3D-weave architecture.

References

[1] S. Kazemahvazi, N. Khokar, S. Hallström, H. Wadley and V. Deshpande. Confluent 3D-assembly of fibrous structures. *Composites Science and Technology*, 127:95-105, 2016.

[2] N. Khokar, F. Winberg, and S. Hallström. Novel 3D preform architecture for performance and reliability of structural beams. *Proceedings of the 20th International Conference on Composite Materials ICCM-20, Copenhagen, Denmark*, July 19-24 2015.

[3] S. Pinho, R. Darvizeh, P. Robinson, C. Shuecker and P. Camanho. Material and structural response of polymer-matrix reinforced composites *Journal of Composite Materials*, 46:2313-2341, 2012.

[4] N. Khokar. 3D-Weaving: Theory and Practice *Journal of the Textile Institute*, 92:193-207, 2001.

[5] T. Ekermann, and S. Hallström. Mechanical characteristation of composites with 3D-woven reinforcement. *Proceedings of the 20th International Conference on Composite Materials ICCM-20, Copenhagen, Denmark*, July 19-24 2015.

[6] L.Brown, M. Sherburn. Texgen v3.9.0, Zenodo (2017). doi:http://doi.org/10.5281/zenodo.291485.

[7] J. Juhasz, R. Rolfes and K. Rohwer. A new strength model for application of a physically based failure criterion to orthogonal 3D fibre reinforced plastics. *Composites Science and Technology*, 61:1821-1832, 2001.

[8] S. Pinho, C. Dávila, P. Camanho, L. Iannucci, and P. Robinson. Failure models and criteria for FRP under in-plane or three-dimensional stress states including shear non-linearity. NASA/TM-2005-213530. NASA Langely Research Center. Hampton, VA 2368, 2005.

[9] E. Greenhalgh. *Failure analysis and fractography of polymer composites*, Woodhead Publishing, 2009.